Electronic Supplementary Material (ESI) for Nanoscale.

SUPPORTING INFORMATION

Supramolecular self-assembly of graphene oxide and metal nanoparticles into stacked multilayers by means of a multitasking protein ring.

Matteo Ardini, Giordana Golia, Paolo Passaretti, Annamaria Cimini, Giuseppina Pitari, Francesco Giansanti, Luana Di Leandro, Luca Ottaviano, Francesco Perrozzi, Sandro Santucci, Vittorio Morandi, Luca Ortolani, Meganne Christian, Emanuele Treossi, Vincenzo Palermo, Francesco Angelucci, Rodolfo Ippoliti

Supporting Figure 1. *Sm*PrxI amino acid sequence engineered with the N-terminal metal-binding sequence. The additional N-terminal sequence is highlighted in grey. Metal binding residues, namely histidine (H) and aspartate (D), are indicated in blue. All the sulphur-containing residues putatively acting in the reduction of GO, *i.e.* cysteine (C) and methionine (M), are indicated in orange.

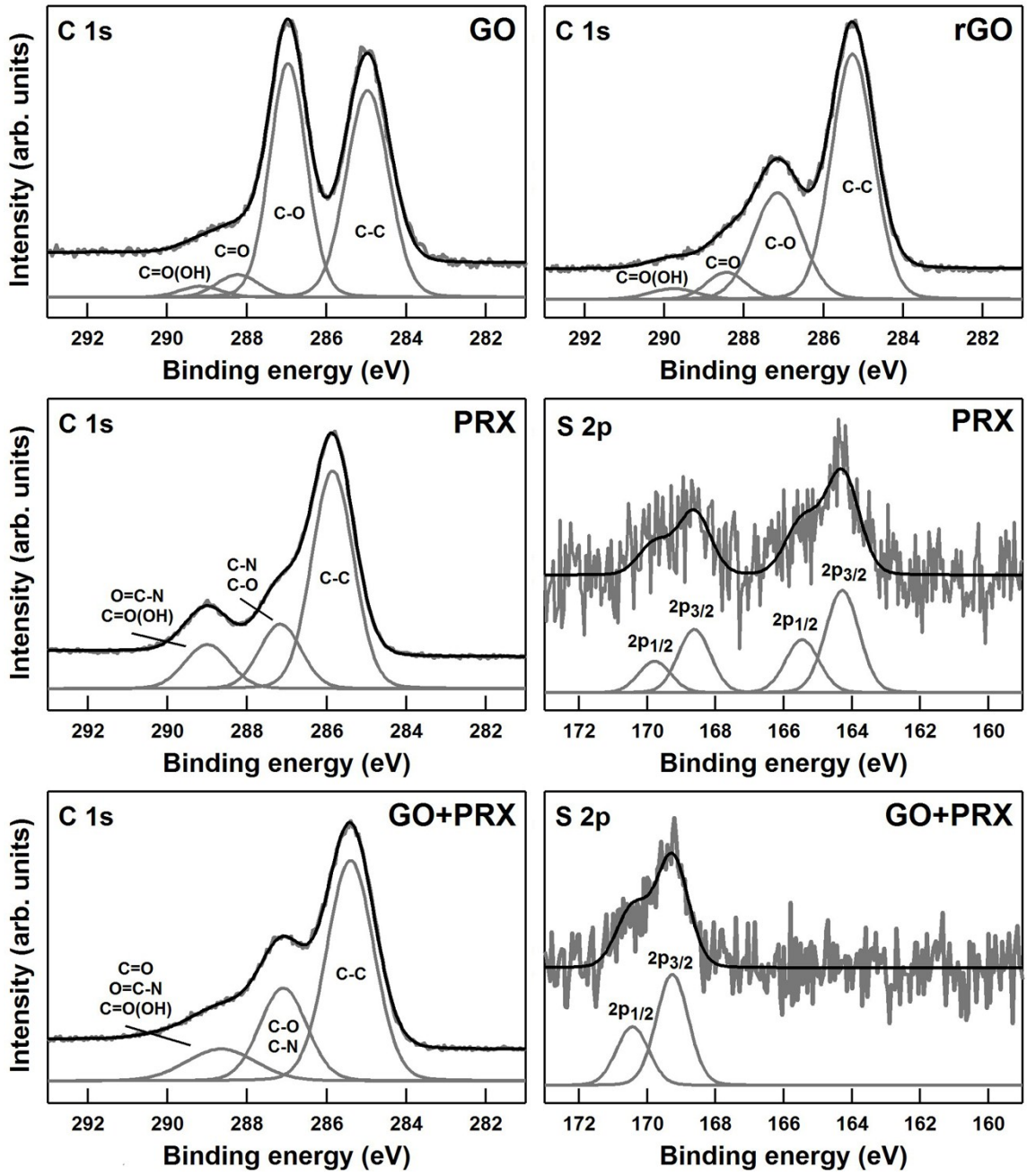

Supporting Figure 2. XPS C 1s and S 2p core level spectra of GO, Prx and GO+Prx. The most relevant chemical information about GO, Prx and GO+Prx can be obtained analysing the XPS C 1s and S 2p core level spectra. The GO C 1s spectrum is characterized by four peaks related to aromatic sp^2 carbon (C–C), epoxy and hydroxyl groups (C–O), carbonyl groups (C=O) and carboxyl groups (C=O(OH)). The Prx C 1s spectrum has been fitted with three peaks assigned to carbon-carbon bonds (C–C), carbon-nitrogen and single carbon-oxygen bonds (C–N/C–O) and double carbon-oxygen bonds (C=O). The spectrum features suggest that the protein is not bounded to the gold substrate [Humblot *et al.*, Langmuir. 2014, 30, 203-12]. The GO+Prx C 1s spectrum has been fitted, for reason of simplicity, with three peaks assigned consistently with the GO and Prx peaks.

The rGO C 1s spectrum has been calculated subtracting from the GO+Prx spectrum the Prx spectrum after a renormalization to the nitrogen signal intensity. Finally the Prx and GO+Prx S 2p spectra have been fitted respectively with two and one doublet related to the 2p orbital spin-orbit coupling. The shift and the relative intensity between the $2p_{3/2}$ and the $2p_{1/2}$ peaks were fixed respectively equal to 1.2 eV and 0.5.

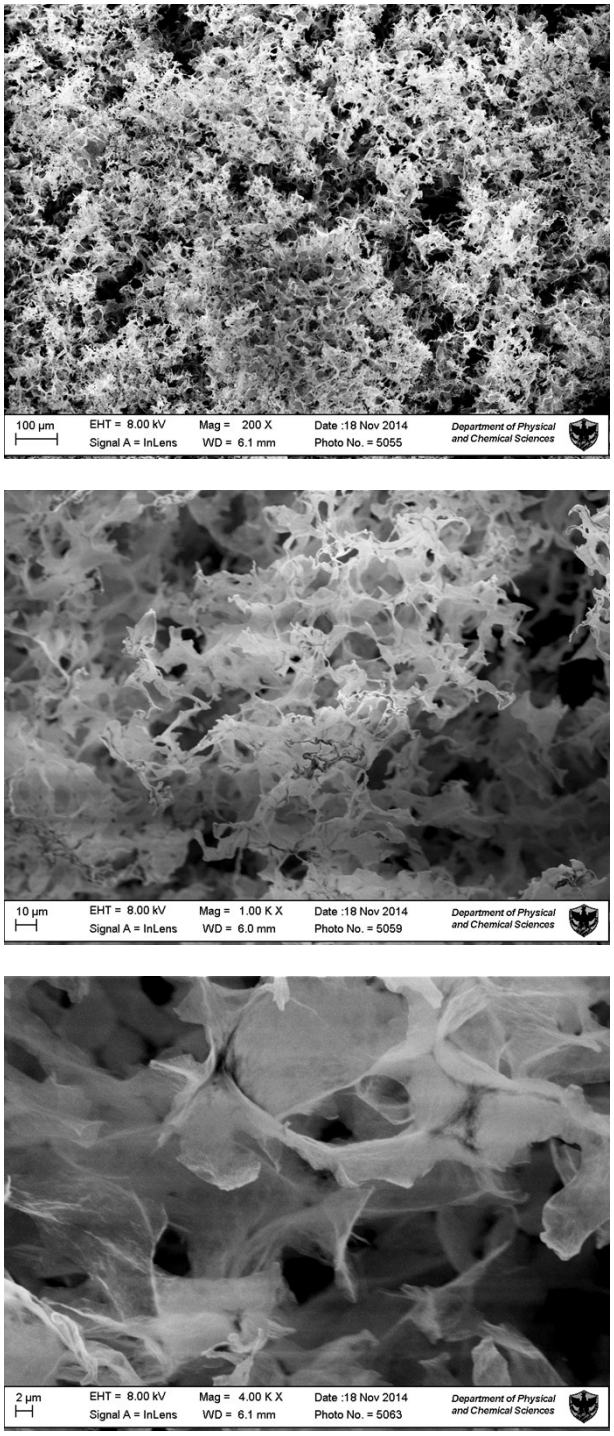

Supporting Figure 3. SEM images of chemically reduced rGO-*Sm*PrxI. Incubation of the rGO-*Sm*PrxI colloid with $NaBH_4$ leads to a fragmented 3D microporous material composed of several multi-layer rGO sheets, hence keeping the architecture of the original colloid. Experimental conditions: 20 mM sodium phosphate buffer pH 7.5; 0.3 mg ml^{-1} GO; 0.6 µM *Sm*PrxI (ring concentration); 15 mM $NaBH_4$; 16 h reduction time; washing with bi-distilled water; 3 h lyophilisation treatment by freeze-drying.

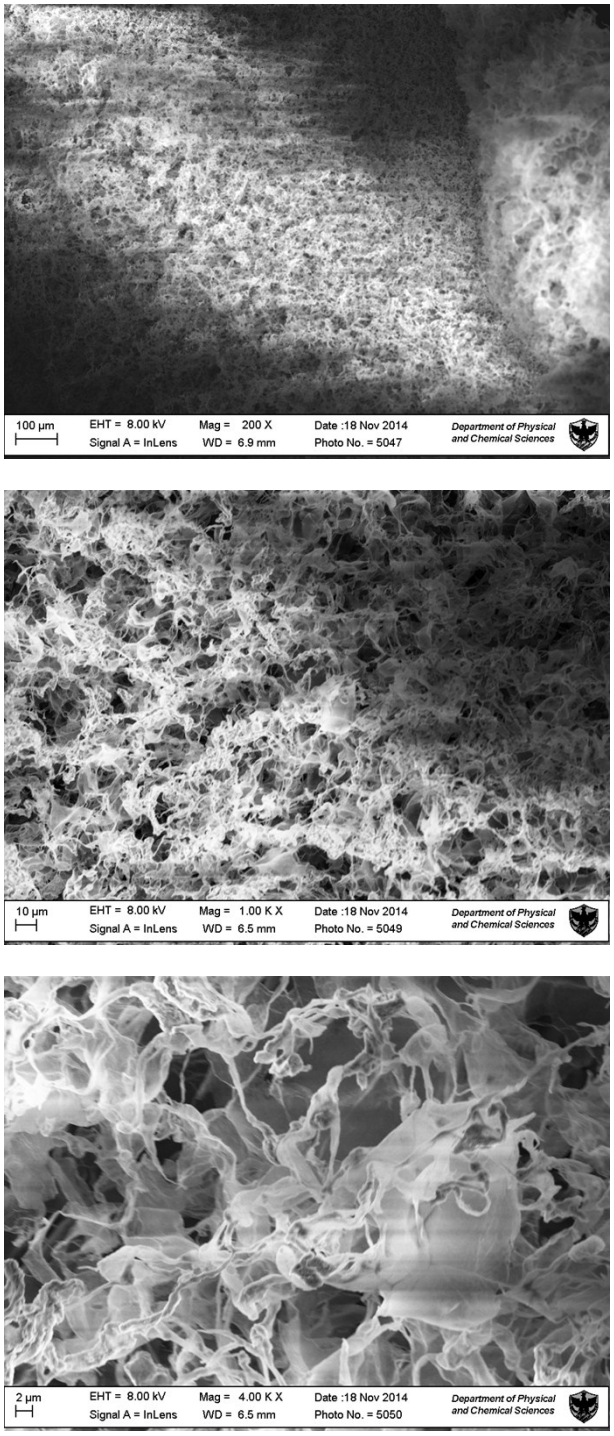

Supporting Figure 4. SEM images of chemically reduced GO. Unlike the unreduced material, chemically reduced GO with $NaBH_4$ forms a fragmented 3D material with internal micro-cavities. However, the resulting architecture is highly disordered and the multi-layer arrangement is less evident. Experimental conditions: 20 mM sodium phosphate buffer pH 7.5; 0.3 mg ml^{-1} GO; 15 mM $NaBH_4$; 16 h reduction time; washing with bi-distilled water; 3 h lyophilisation treatment by freeze-drying.

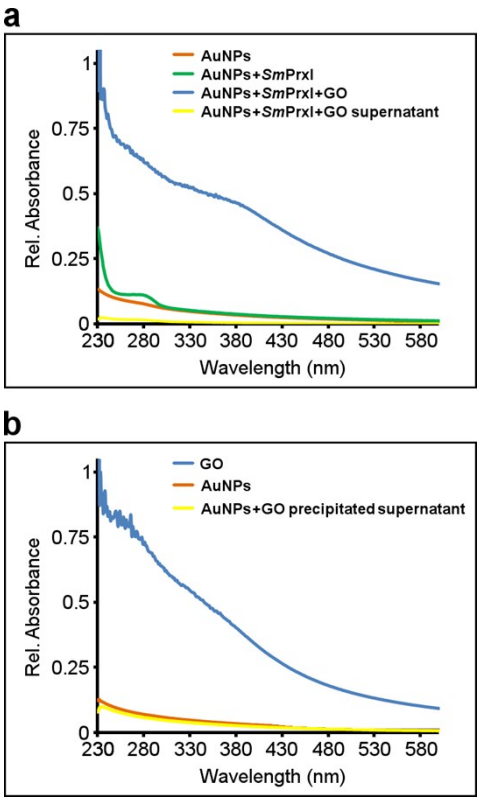

Supporting Figure 5. *Sm*PrxI-mediated adsorption of AuNPs on rGO. a) AuNPs are easily dissolved in aqueous buffer containing imidazole together with *Sm*PrxI. The mix shows a wide optical absorbance due to the gold matter and peaks at 230 and 280 nm typical of the proteins. The addition of GO causes increase of the signal and the resulting rGO-*Sm*PrxI-AuNPs undergoes clumping to form a colloidal hydrogel after approximately 60 min (data not shown). Precipitation collects all the components within the colloid making the supernatant almost completely clarified showing zeroed absorbance. b) A control protein-free experiment proves the role of *Sm*PrxI acting as a sticky moiety to induce aggregation of GO and attach the AuNPs onto it. In fact, in the absence of protein the AuNPs are not effectively bound to GO such that they can be quickly separated by ultracentrifugation and in the presence of salts (50 mM NaCl) which induces GO gelation and precipitation.

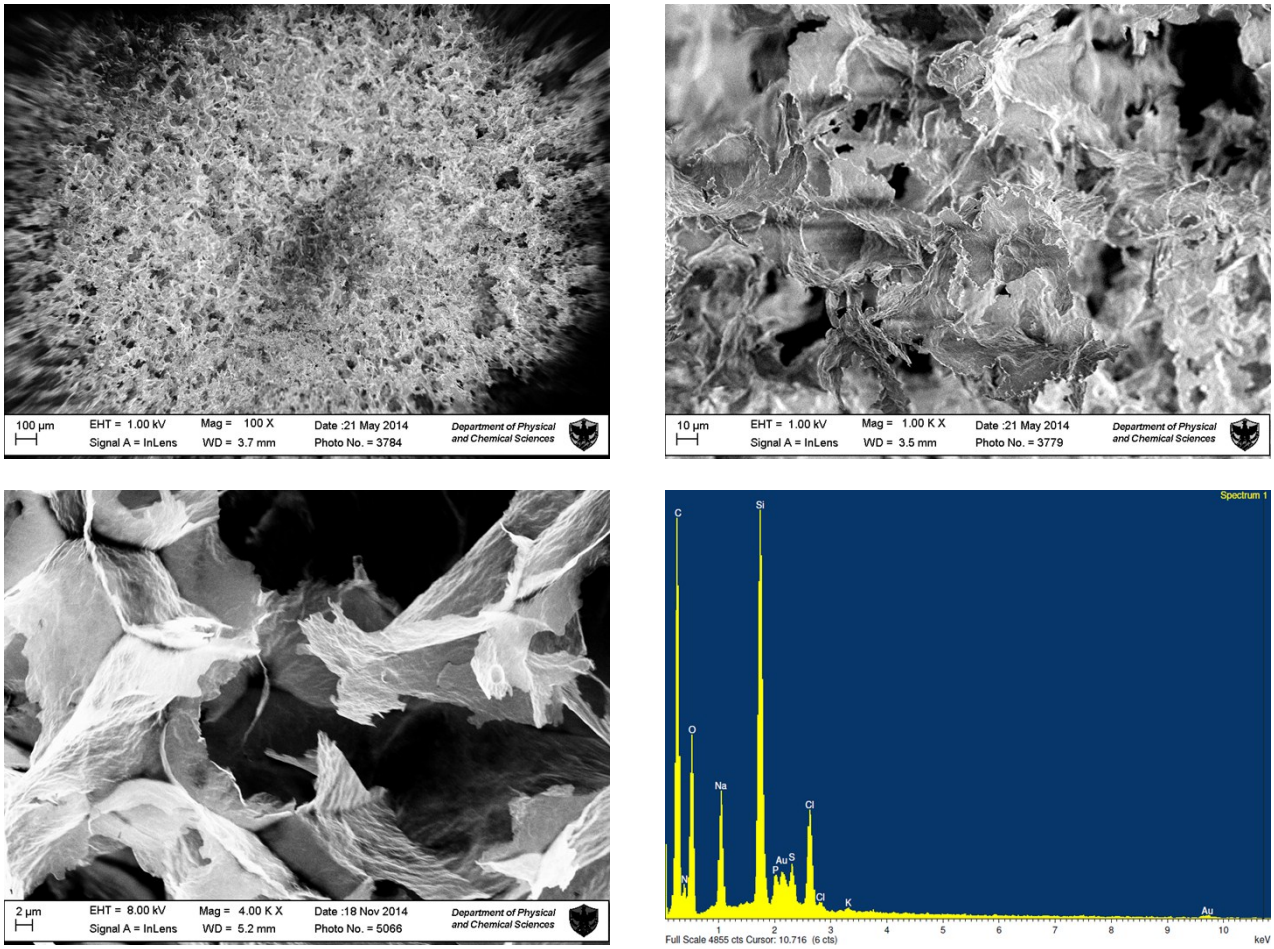

Supporting Figure 6. SEM images and EDS analysis of rGO-*Sm*PrxI-AuNPs. As for the rGO-*Sm*PrxI material, a 3D microporous organization made by several cross-linked multi-layer rGO sheets is observed, hence retaining the architecture of the original colloid. Experimental conditions: 20 mM sodium phosphate buffer pH 7.5; 0.3 mg ml^{-1} GO; 0.6 µM *Sm*PrxI (ring concentration); 0.6 µM AuNPs; washing with bi-distilled water; 3 h lyophilisation treatment by freeze-drying.

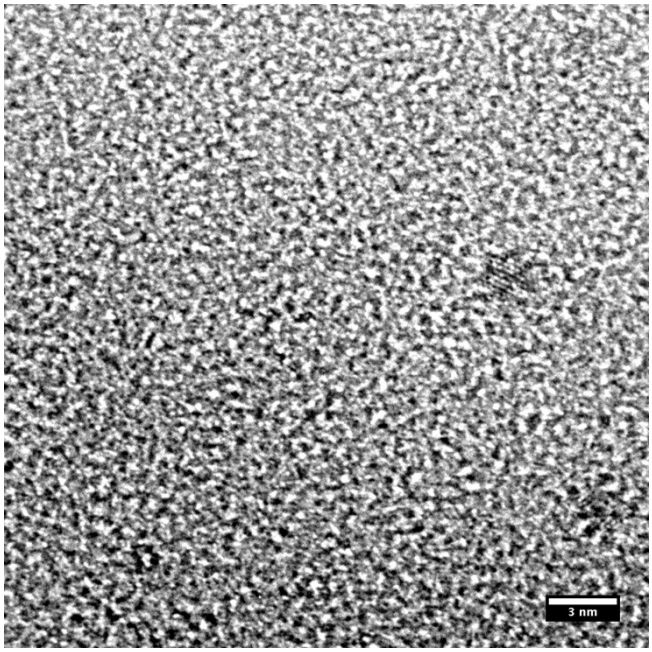

Supporting Figure 7. HRTEM micrographs of commercial Ni^{2+}-functionalized AuNPs.

Micrographs confirm the presence of crystalline nanoparticles, compatible with gold crystal phase, showing 0.235 nm spaced lattice fringes.

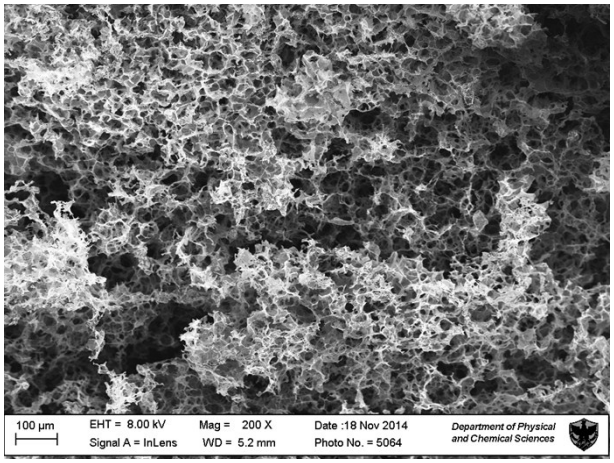

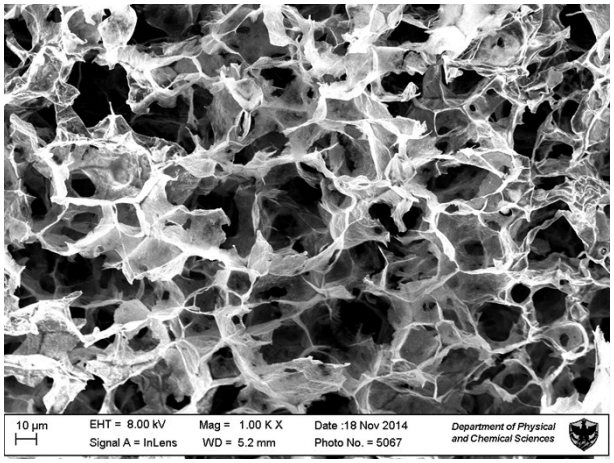

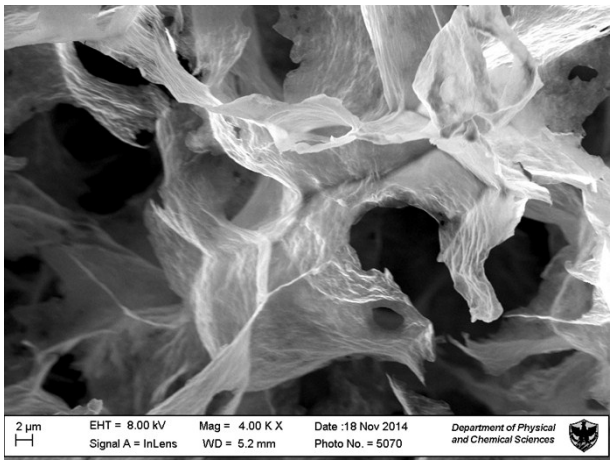

Supporting Figure 8. SEM images of chemically reduced rGO-*Sm*PrxI-AuNPs. As for the unreduced material (see Supporting Figure 6), this hybrid retains the ordered microporous architecture without loss of the multi-layer arrangement. Experimental conditions: 20 mM sodium phosphate buffer pH 7.5; 0.3 mg ml^{-1} GO; 0.6 µM *Sm*PrxI (ring concentration); 0.6 µM AuNPs; washing with bi-distilled water; 3 h lyophilisation treatment by freeze-drying.

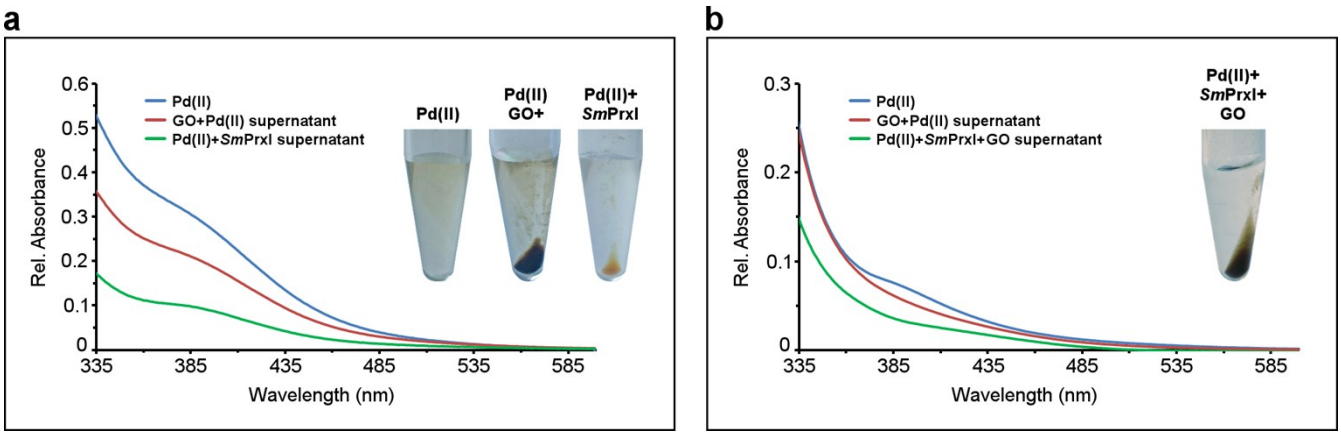

Supporting Figure 9. Pd^{2+} adsorption by *Sm*PrxI and GO. a) Pd^{2+} in buffer appears as a pale yellow solution giving a characteristic absorbance signal upon reaction with TGA. After mixing with *Sm*PrxI, the solution clumps into a yellow pellet and the resulting supernatant reacts with TGA providing ~60% quenched signal meaning that a large amount of Pd^{2+} ions precipitated into the pellet, presumably with the protein. Even after washing the pellet, no significant absorbance is recorded, suggesting that Pd^{2+} and *Sm*PrxI strongly interact. In a control assay, when Pd^{2+} is mixed with GO a dark brown pellet is collected and ~20% quenched signal is observed upon reaction of the supernatant with TGA. However, after washing most of the lost signal is recovered indicating that, unlike *Sm*PrxI, GO cannot stably hold Pd^{2+} by itself (data not shown). **b)** The *Sm*PrxI-Pd^{2+} conjugates remain stable with imidazole and trigger the formation of a 3D hydrogel after mixing with GO. When assessing the supernatant through the TGA-Pd^{2+} assay about 50% absorbance decrease of the 383 nm reference signal is observed indicating that ~800Pd^{2+} ions were stably trapped within the colloid even after washing, thus suggesting that *Sm*PrxI can load Pd^{2+} while keeping its sticking behaviour towards GO. In the absence of protein only weak absorption of Pd^{2+} by GO is recorded.

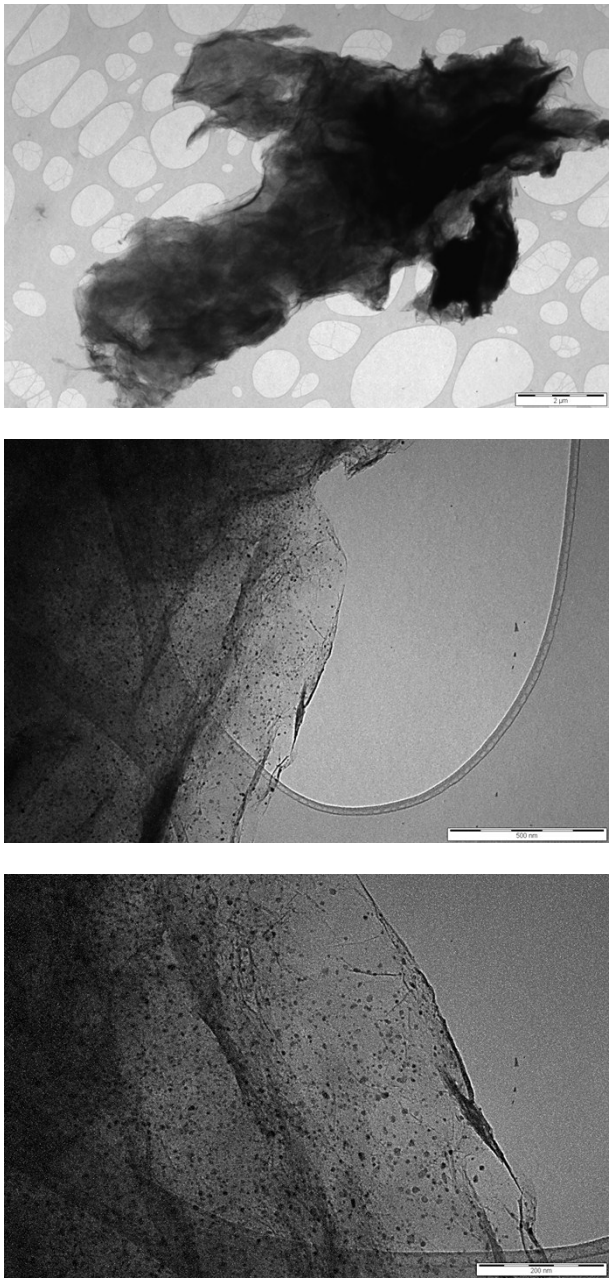

Supporting Figure 10. TEM micrographs of chemically reduced rGO-*Sm*PrxI after interaction with Pd^{2+}. The multi-layer 3D rGO composite formed upon mixing with *Sm*PrxI retains its ability of stably capturing Pd^{2+} in solution. Thus, after chemical treatment with $NaBH_4$ the material forms amorphous structures showing very high electron density indicating the presence of metal inside. High magnification reveals the presence of PdNPs spread over the surface, hence proving the ability of the preformed rGO-*Sm*PrxI complex to capture metal ions.